Phase II STTR: Experimental Studies of JTECH Power Generation in a Scramjet

J. Berlette, D. Scarborough, S. Menon
School of Aerospace Engineering
Georgia Institute of Technology, Atlanta, GA

Phase II Subcontract Final Report
JEMS-2010-004-01
Under Prime Contract
FA9550-11-C-0004

Submitted to

Johnson Research and Development Company
Atlanta, GA
And
US Air Force Office of Scientific Research
Washington DC

March 6 2013

Contents

1 INTRODUCTION

This report constitutes a fulfillment of Georgia Tech's responsibilities in the Johnson Thermoelectric Energy Converter (JTEC) project. In Phase I and the first part of Phase II, student researchers at GT's Ben T Zinn Combustion Lab (hereafter the Combustion Lab) carried out an analysis of the thermodynamics of the proposed JTEC device as if it was placed in the walls of the combustor of a supersonic combustion ramjet. Next, the device was to be tested in the supersonic combustion wind tunnel at the Combustion Lab. Because the proposed device was too large to fit in the wind tunnel, a test bed was built to simulate the pressures and temperatures required. Unfortunately, no JTEC devices were supplied by Johnson Electro-Mechanical systems. This report will be a review of the design, construction and operation testing of the test bed before the termination of this project.

2 PHASE I: JTEC FEASIBILITY FOR SCRAMJET OPERATION

2.1 Literature Survey

In phase I Georgia Tech researchers assembled a literature review, which could help identify sources of waste heat in a typical scramjet. The leading edges and control surfaces of the aircraft were examined as possible sources of waste heat, but it was confirmed that the combustor of the engine was the only source of the most stray heat.

2.2 Preliminary Analysis

A preliminary thermodynamic analysis was done to determine some basic characteristics of a scramjet engine.

The inlet conditions at a flight altitude of 90,000 ft were assumed to be the ambient properties of air from standard atmosphere, i.e., pressure of 0.250 psi and temperature of 224 K. The properties of the flow at the exit of the inlet were taken from fore-body and inlet design test of the HiFire engine. These properties were an inlet Mach number of 3.42 at a pressure of 13.8 psi, temperature of 905.5 K, and a mass flow rate of 4.21 lb/s.

Assuming an adiabatic isolator, the combustor entrance conditions were taken to be the same as those of the inlet exit. These properties were fed into the chemical equilibrium program GasEq, which calculated the adiabatic flame temperature and the product composition. Assuming a perfectly expanded nozzle and isentropic flow expansion, the thrust and other performance parameters were calculated. The engine produced approximately 2,950 N of thrust during its operation. Finally, the heat added during combustion and heat rejected at the exhaust was calculated to be 2,636 kJ/kg and 1,342 kJ/kg, respectively, yielding a cycle work of 1,294 kJ/kg.

2.3 Scramjet Cycle Analysis

A 1-D cycle analysis was performed on a model scramjet engine, based on the Air Force Research Lab's HIFiRE engine. The overall thrust produced during flight, and the temperatures and pressures of the different components of the engine were determined. The heat loss in each component of the engine was calculated, and the effect on the engine's specific thrust was found. The effect of the heat loss was used to determine the impact a device such as JTEC would have on an engine's performance. The analysis was done for a hypersonic vehicle travelling at Mach 8.0 at 90,000 ft. Figure 1is a sketch of the engine model.

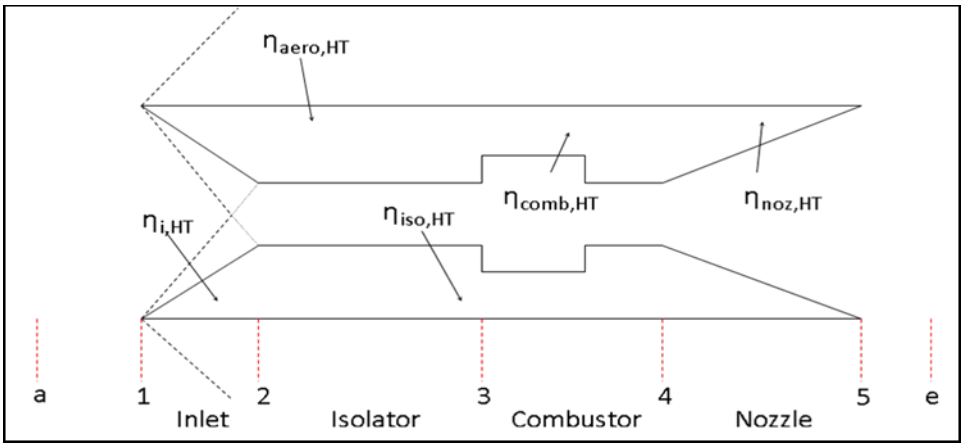

Figure 1: Scramjet model.

The 1-D cycle model was implemented in MATLAB. The program was capable of computing the thrust, the heat loss through the combustor wall, and the overall efficiency of the engine. A flow chart of the program can be seen in Figure 2.

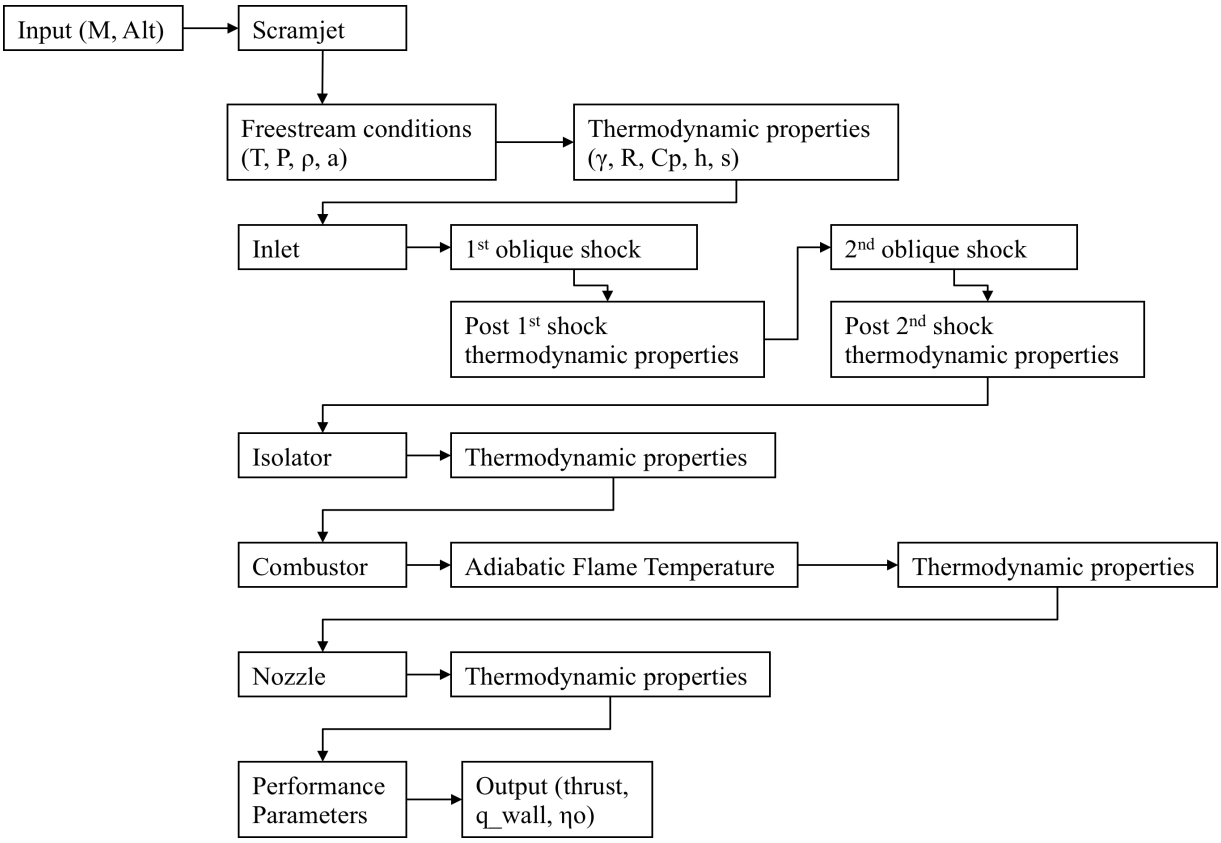

Figure 2: Flowchart of 1-D Scramjet Engine Model

From the input Mach number and altitude, the program calculated freestream conditions from the U.S. standard atmosphere, and the thermodynamic properties for the air from NASA polynomials. The model assumed that there were two oblique shocks in the inlet, one to turn the flow and the other to straighten it into the isolator. The properties after the shocks were easily calculated.

Given an isolator with specified heat transfer efficiency, the combustor entrance conditions were taken to be those of the exit inlet minus the loss experienced in the isolator. In the combustor, a subroutine solved for the adiabatic flame temperature and equilibrium composition given a fuel (in this case, ethylene) and fuel-to-air ratio. A combustion efficiency factor was also introduced in the heat release calculations, which accounted for the fact that some of the chemical energy in the fuel may not be released due to inadequate mixing or reaction time. Heat losses were then accounted for at the start of the nozzle by varying the heat loss efficiency before the flow was allowed to adiabatically expand in the nozzle. Assuming an ideally expanded nozzle, the exit velocity, thrust, and other performance parameters were calculated. Figure 3 is a temperature-entropy plot of the cycle.

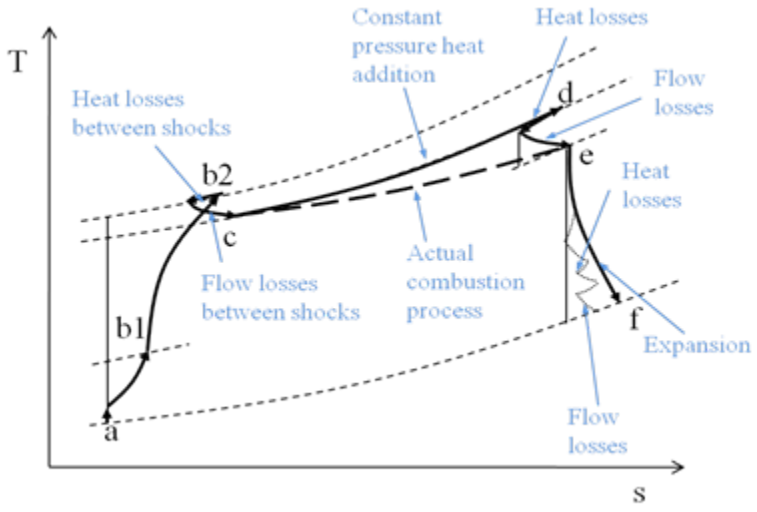

Figure 3: Temperature-Entropy diagram of scramjet cycle

The developed model was used to predict the effect of extracting combustor heat for power generation on scramjet specific thrust. For the baseline case, i.e., no waste heat, the engine thrust and overall cycle efficiencies were calculated to be 2,950 N and 0.49, respectively.

These calculations were repeated for values of nozzle heat transfer efficiency ranging from 0.5% to 25% and for the flight Mach numbers and altitudes of interest. Figure 4 shows the available nozzle waste heat at the desired range of Mach numbers. For a fixed heat transfer efficiency, the rate of increase of heat flux with Mach number increases for higher Mach numbers. Figure 5 is a plot of the specific thrust versus Mach number. Based on this analysis, the specific thrust decreases with increasing Mach number and is relatively insensitive to changes in the nozzle heat transfer efficiency, indicating that for a given flight Mach number the heat losses in the nozzle do not significantly affect specific thrust.

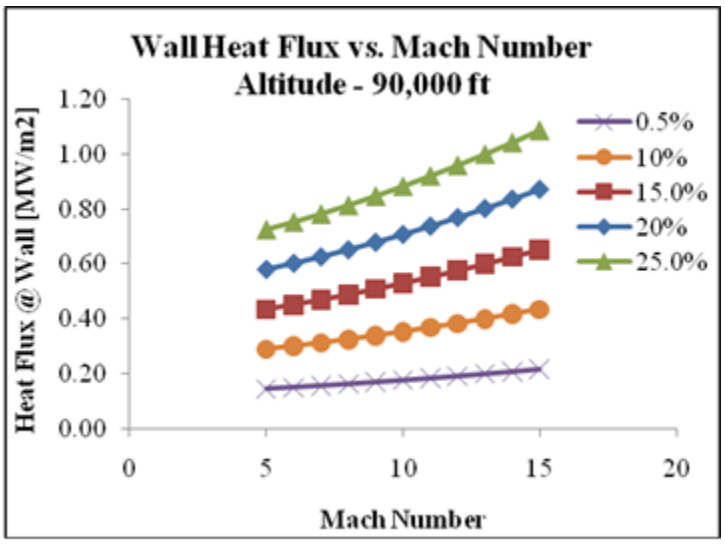

Figure 4: Nozzle heat flux versus Mach number

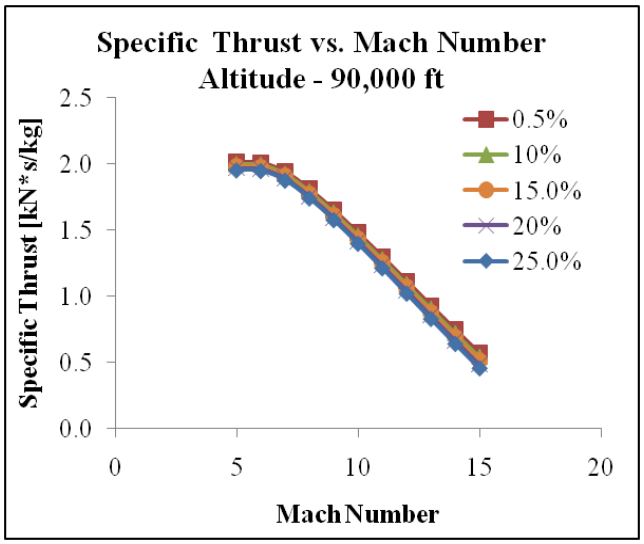

Figure 5: Specific thrust as a function of Mach number for various heat loss efficiencies.

2.4 1-D Combustor Heat Transfer Model

A better idea of what the temperatures and the heat flux in the combustor was desired to determine the optimum location for the JTEC cells. This section describes the basic methodology for estimating the steady-state heat flux to the cavity floor, forward facing step, and the top of the ramp in the scramjet test facility. A schematic of the physical situation is shown in Figure 6, along with the relevant velocities and temperatures used in this analysis.

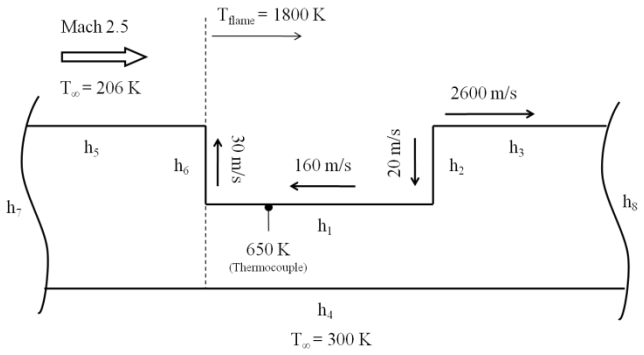

Figure 6: Schematic of the scramjet combustor.

Both experimental and computational fluid dynamics data were used to determine the scramjet cavity gas properties. The measured static pressure and Mach number in the combustor were 85

kPa and 2.5, respectively. The velocity field in the cavity was obtained from the scramjet CFD results by Choi et. al.[2]

The measured temperatures of the combustor inlet air flow and of the cavity floor were 206 K and 650 K, respectively. The top of the ramp was initially estimated to be at 1650 K, and the temperature of the back wall of the cavity was assumed to be the average of the floor and ramp temperatures. The mean cavity gas temperature estimated from the CFD results shown in Figure 7 was found to be 1800 K.

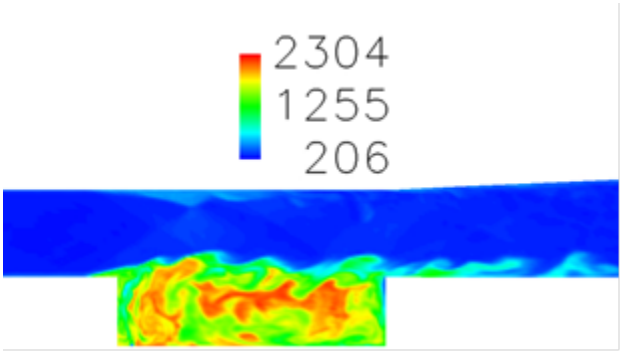

Figure 7: Temperature distribution of cavity from CFD data.[2]

Heat is transferred by convection and radiation from the reacting flow to the step. The convective heat transfer coefficient is difficult to fix precisely due to the uncertain nature of the flow field. The convective heat transfer rate coefficients were obtained from correlations for compressible turbulent flow over a flat plate.[3-7]. The convection coefficients and wall heat fluxes for the scramjet sections are shown in Table 1. The numbers in the top row correspond to the stations shown in Figure 6. These results indicate that the top of the ramp had the highest convective heat transfer coefficient and waste heat.

Table 1: Heat loss through different sections of combustor.

	1	2	3	4	5	6	7	8
h_{avg} (W/m^2 K)	88.18	15.92	501.55	389.57	514.88	22.57	32.65	25.81
$q_{w,\,avg}$ (kW/m^2)	115.97	11.67	851.28	56.52	128.33	16.55	12.35	22.40

2.5 ANSYS Model of Combustor

Next, ANSYS was used to predict the two-dimensional, steady-state heat flux $q''(x, y)$ and temperature distribution $T(x, y)$ on the step and side walls of the combustor. Boundary conditions, convective heat transfer rate coefficients, and wall material properties were specified and the ANSYS solver was used to determine both the wall temperature and the heat flux rate.

The ANSYS predicted temperature and heat flux distributions are shown in Figure 8 and Figure 9. The ANSYS predicted temperature at the location corresponding to the thermocouple in the experimental rig was 656 K, which is very close the recorded temperature of 650 K. Also, the ANSYS model predicted the cavity trailing edge temperature to be 1422K, which compared favorably with the estimated 1650 K.

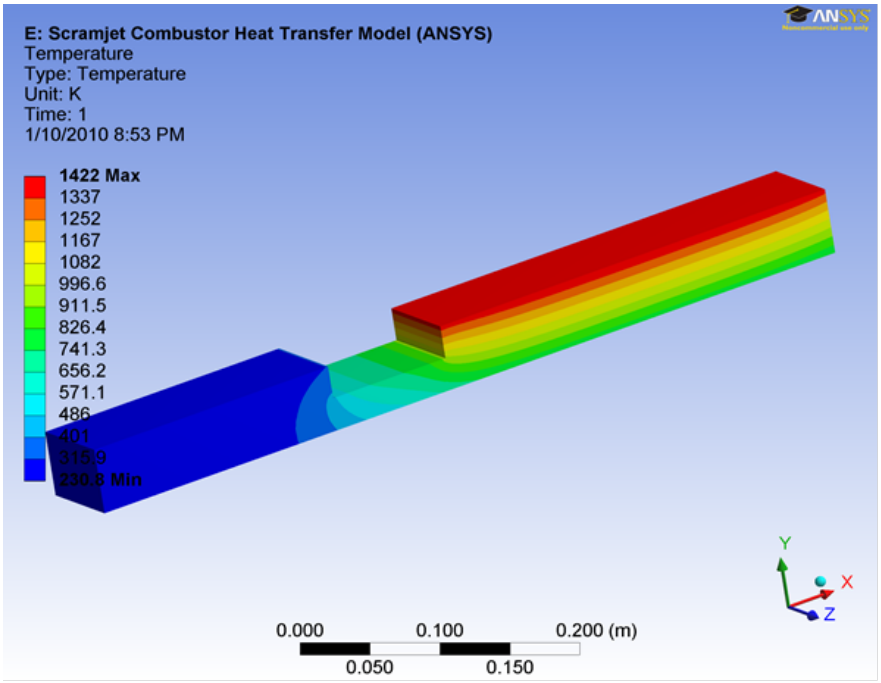

Figure 8: Temperature distribution in scramjet combustor (flow is from left to right).

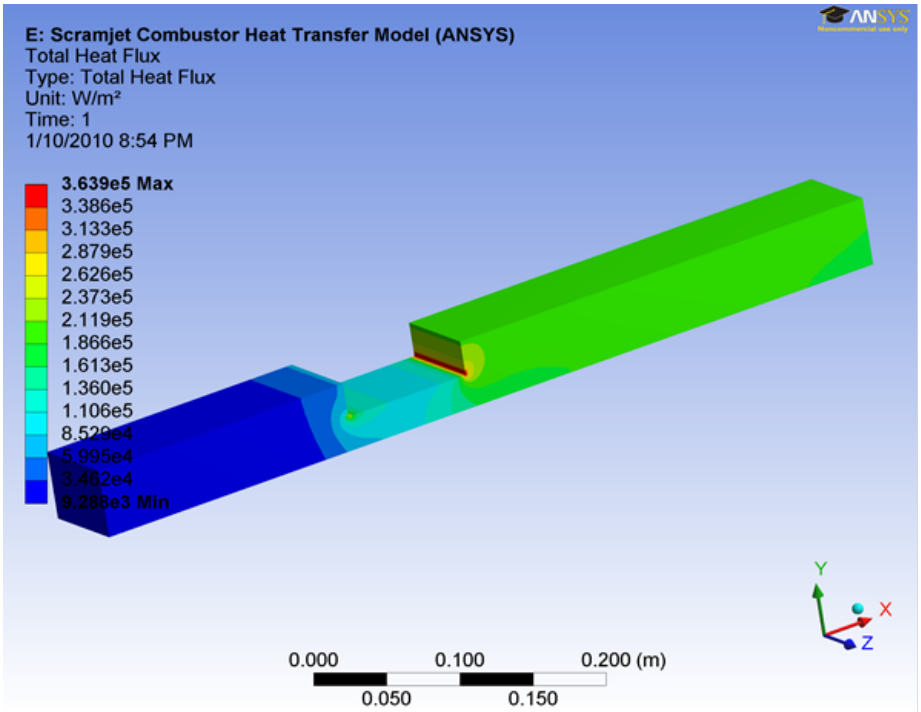

Figure 9: Heat transfer in combustor cavity.

Figure 9 shows that the maximum heat flux was located at the bottom of the cavity, closer to the trailing edge. The heat flux predictions from the reduced-order model in Table 1 agreed well with those from the ANSYS model. In both cases, the waste heat transfer available for power generation was on the order of 10^5 W/m2. Therefore, the bottom of the cavity and the top of the ramp were deemed promising locations for testing the JTEC system.

2.6 Temperature Measurements in Scramjet Ground Test Facility

Experimental data was desired to validate the temperatures and heat transfer rates in the combustor of the scramjet. The Georgia Tech Supersonic Combustion Test Facility is shown in Figure 10. It is a blowdown tunnel, fed by the Combustion Lab's high pressure air tanks. During operation, heated air flows through the supply pipe (1), into the stagnation chamber (2). From there, it continues on through a flow-conditioning section (3) into the combustion section (4).

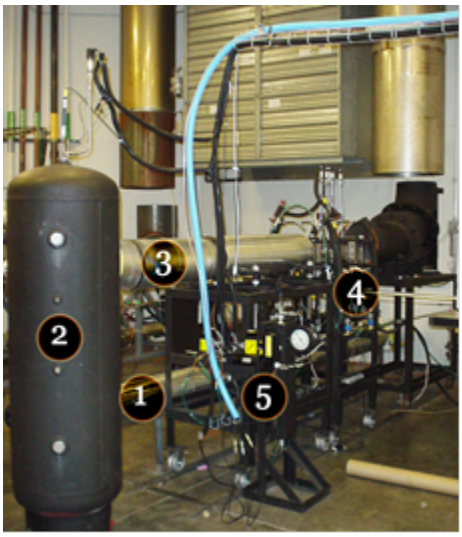

Figure 10: Photo of scramjet ground facility

The test section is contained in a 635 mm x114.5 mm x 133.5 mm, 316 stainless steel block as shown on Fig. 9. The boundary layer compensated nozzle provides an air flow of 3 kg/s, at Mach 2.5, which enters shock-free into a 31.75 mm x 63.5 mm, rectangular test section.

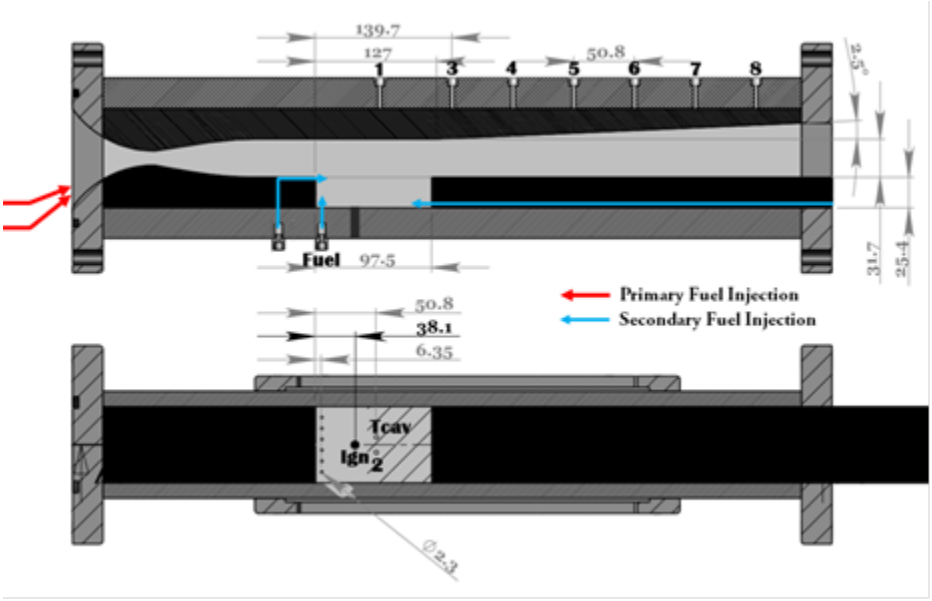

Figure 11: Scramjet ground facility test section.

The cavity's L/D ratio is adjustable from 0 to 5 by moving the aft floor. Six span-wise, equally spaced, 2.3 mm diameter fuel injectors are located in the leading step, on the floor, and in the aft step of the cavity. Quartz windows close the combustor sides and top to allow for flow visualization.

Eight 3.125 mm, K-type thermocouples are located in the 406 mm x 63.5 mm x 25.4 mm aft floor ramp as shown in Figure 12. Wall heat flux can be estimated from the temperature gradients calculated from the measured temperatures at known locations.

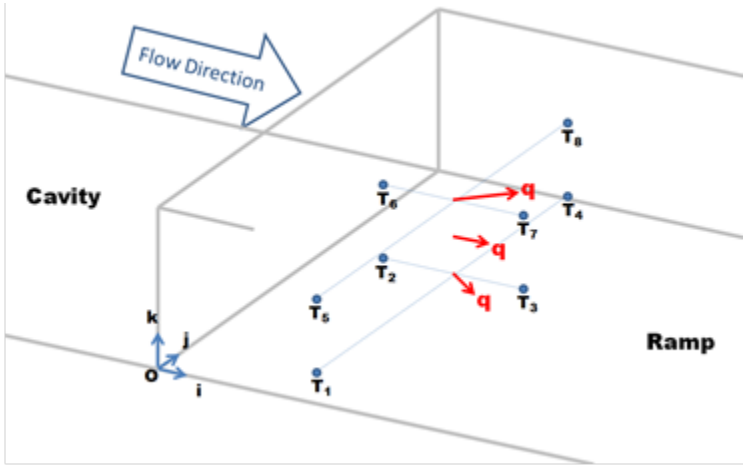

Figure 12: Thermocouple locations in scramjet test section.

A series of combustion tests with "in cavity burning" as shown in Figure 13 were conducted to determine the ramp temperature and heat flux using a jet-A surrogate mixture of 65% ethane and 35% methane. During these tests, the stagnation pressures and temperatures were 13 MPa and 305 K, respectively. The air mass flowrate was 2.2 kg/s. The measured combustor static pressure was 85 kPa and 70 kPa with and without combustion, respectively.

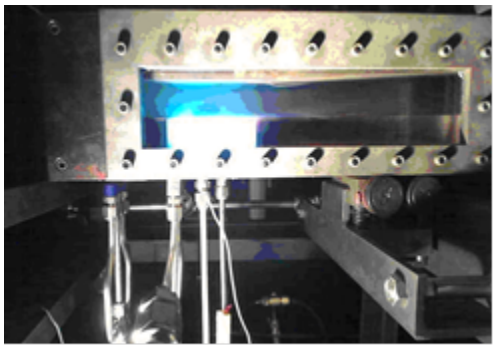

Figure 13: In-cavity burning.

Figure 14 shows transient temperature data at three locations in the step, 748 s after ignition. Steady-state operation was achieved after one minute, and a blow-off event was simulated by cutting off the fuel supply at t = 830 s. The average heat flux computed from the temperature

measurements was 0.16 MW/m^2. This is consistent with the predicted heat flux obtained in the numerical analysis.

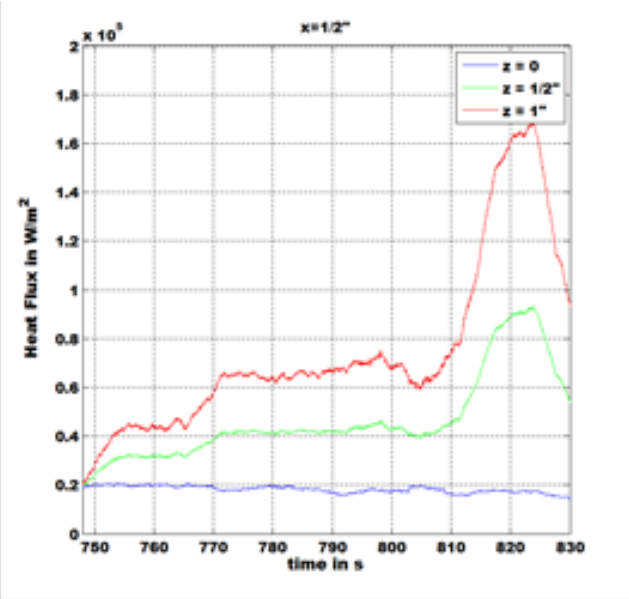

Figure 14: Heat flux in combustor, steady state and blow-out.

3 PHASE II OBEJCTIVES AND WORK PLAN

It was found that the prototype fuel cells being developed by Johnson Electromechanical were too large to fit in the Combustion Lab's supersonic combustion wind tunnel. It was decided to make a testing rig especially for them. The conditions that were desired for the test were a temperature of 1000K and a pressure of 300 psi. The temperature was taken from the ANSYS simulations and experimental data of the supersonic cavity combustor. It was close to the temperature at the trailing corner of the cavity combustor, seen in Figure 8, earlier.

The pressure that this test bed would be able to reach was limited by the materials in the pressure vessel. The hot parts of the rig were originally to be made using 304 stainless steel, which was not recommended above 870 degrees Celsius (1143 K). The temperature affects the strength of the steel, and therefore its ability to maintain its shape under pressure. A conservative design point of 300 psi (~20 atmospheres) was therefore chosen.

3.1 The Fuel Cells

The device that was shown to Georgia Tech was a solid oxide fuel cell. It was a ceramic tube, 3/8th's of an inch in diameter and 6 inches long. A material was painted on the inside and outside tip of the tube. The cell required a hot, oxygen-rich environment on one side, and an oxygen-

poor one on the other. By introducing this concentration gradient, oxygen anions would flow across the ceramic electrolyte. To produce this gradient, methane was to be passed through the inside of the tube, and hot air over the outside.

In addition to simulating the conditions in supersonic flight, a high temperature and pressure was needed for the fuel cells to produce electricity. By increasing the pressure, the concentration of oxygen on the hot air side will increase, which would improve the power density of the cells. A high temperature was also needed; the ceramic had to be at a very high temperature for it to become electrically conductive.

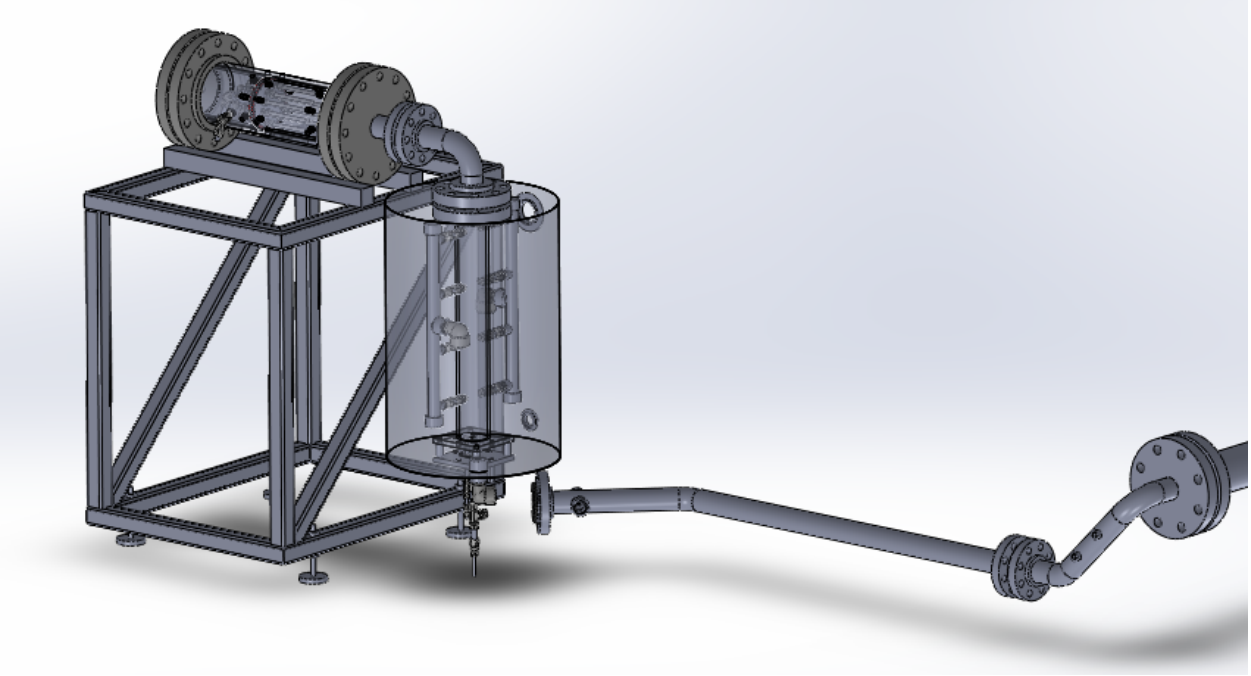

Figure 15: Model of fuel cell testbed.

3.2 Fuel Cell Vessel

The fuel cells were to be held in a pressure vessel which could separate the oxygen-rich and oxygen-poor air that the fuel cell was to be exposed to. Figure 16 is a model of the pressure vessel.

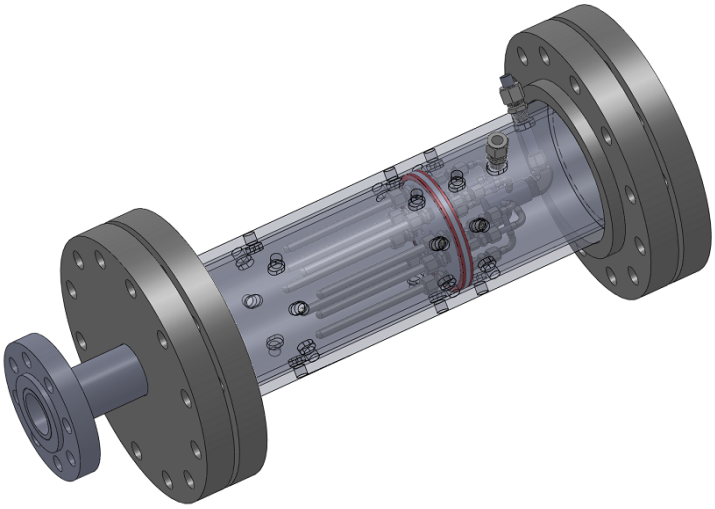

Figure 16: Isometric view of fuel cell vessel.

The long, thin tubes arrayed in the vessel are the fuel cells. They were to be held, by compression fittings, to a plate. This plate was wedged between two sections of pipe that fit within the outer pipe and flanges. The outside flanges provided the compression that kept the assembly together and relatively leak proof. The entire assembly was 304 stainless steel.

Figure 17 is a labeled view of the model. The hot air entered through a large pipe in one of the flanges of the pressure vessel. The hot air would then flow down the length of the fuel cell, and out of a ring of orifices at the base of the cells.

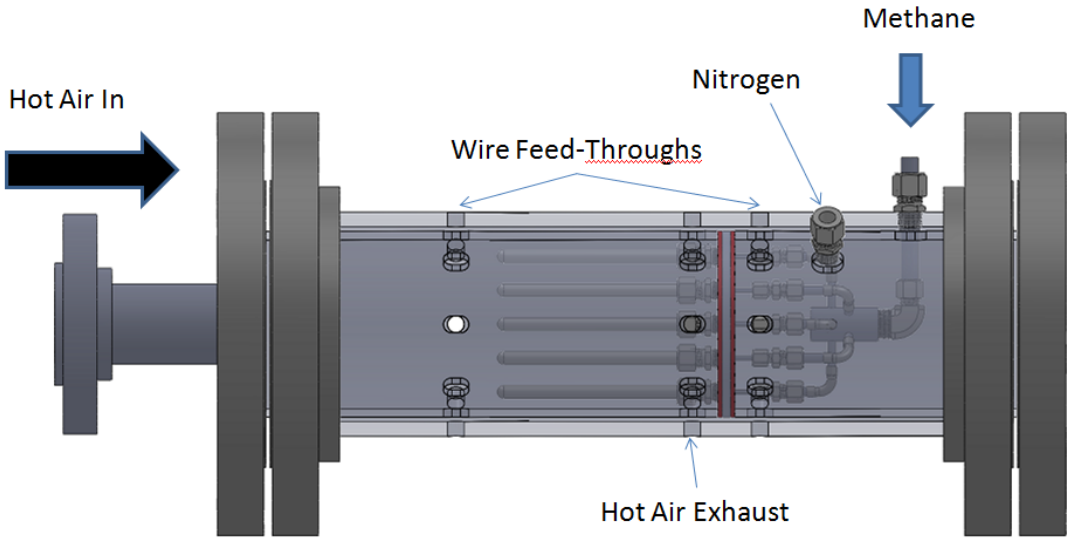

Figure 17: Labeled view of fuel cell vessel.

On the oxygen-poor side, methane was to be sent directly to the inside of the tube via a small manifold, which can be seen in Figure 18. The manifold, of all stainless steel construction, is very compact. The manifold was to be connected to ceramic tubes, which would deliver the methane to the inner tip of the cells. From there, methane would flow out the base of the tubes, and be diluted by a large amount of nitrogen. The nitrogen was added to reduce the possibility of an explosion in the vessel.

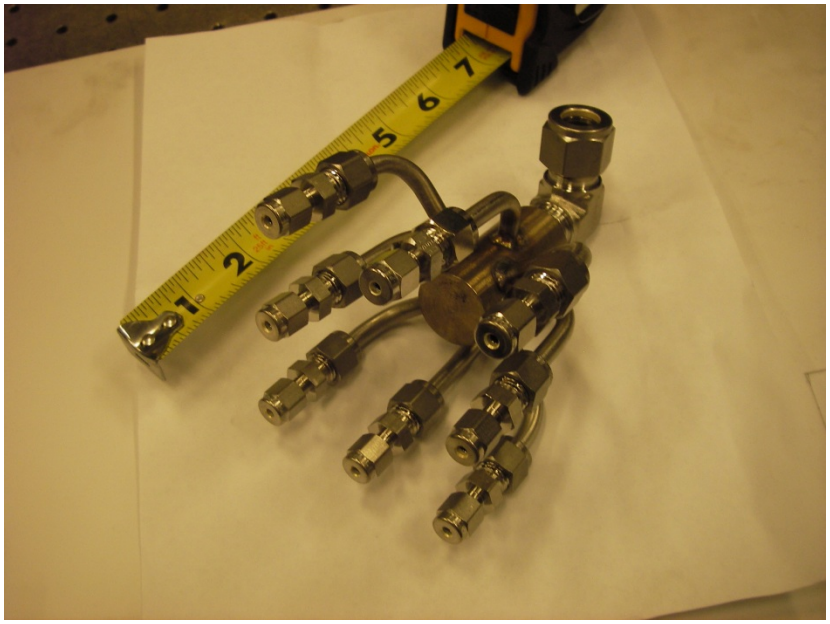

Figure 18: Manifold for fuel cells.

The remaining holes were for the anode and cathode wires of the fuel cells. These wires were to be platinum, to better resist corrosion in the oxygen-poor and oxygen-rich environments. They were to be passed through ceramic tubes, and plugged with ceramic paste.

3.3 Vitiator

Reaching 1000 Kelvin in the pressure vessel was the primary technical hurdle for the test bed. Electric heaters that could produce the necessary power and endure the desired pressures were few, and very expensive. It was decided to vitiate the air instead.

A vitiator is a burner whose products are mixed with the flow that is to be heated. The word “vitiate” means to impair the quality of, or corrupt. A vitiator corrupts a flow by adding products of its combustion and consuming the oxygen that is supplied to it. In order to maximize the concentration of oxygen in the gas on the oxygen-rich side of the cells, it was decided to use an oxy-fuel burner. The fuel was natural gas, which was supplied by the Combustion Lab’s high pressure natural gas system.

The burner itself is a swirler, shown in Figure 19. In this type of burner, the fuel travels through the center tube, and the oxidizer through the outer one. The reactants are then partially mixed by the flutes.

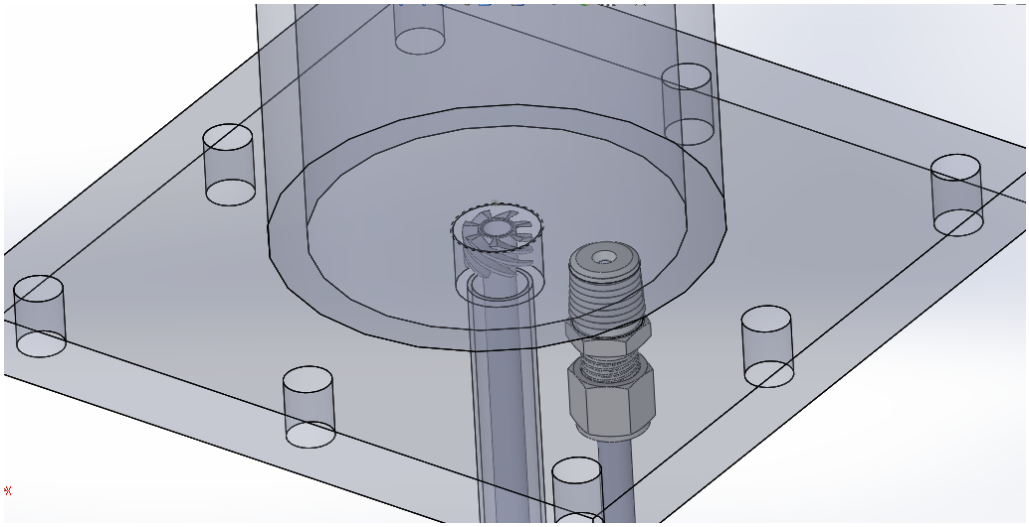

Figure 19: Burner and igniter inserted into bottom plate of vitiator.

The vitiator is a 3 foot long, vertical, stainless steel tube, with the burner inserted into the base. Figure 20 is a photograph of the vitiator. A hydrogen pilot flame/igniter is placed slightly to the side of the burner. Air is brought in by two steel "rails" located alongside the vitiator. The air is brought in stages, in order to avoid quenching the carbon monoxide in the products and lowering the heat extracted from the combustion.

Figure 20: Vitiator

The hydrogen pilot flame is used as a sure-fire way to ignite the burner. Hydrogen is flowed through a tube, around another, ceramic tube which contains a metal rod. An ignition transformer delivered 10,000 volts to the metal rod, where it arced across the exit of the hydrogen tube. This created a stable flame to anchor the oxy-fuel burner. A picture of the hydrogen pilot in operation can be seen in Figure 21. The small blue dot is the spark from the ignition transformer.

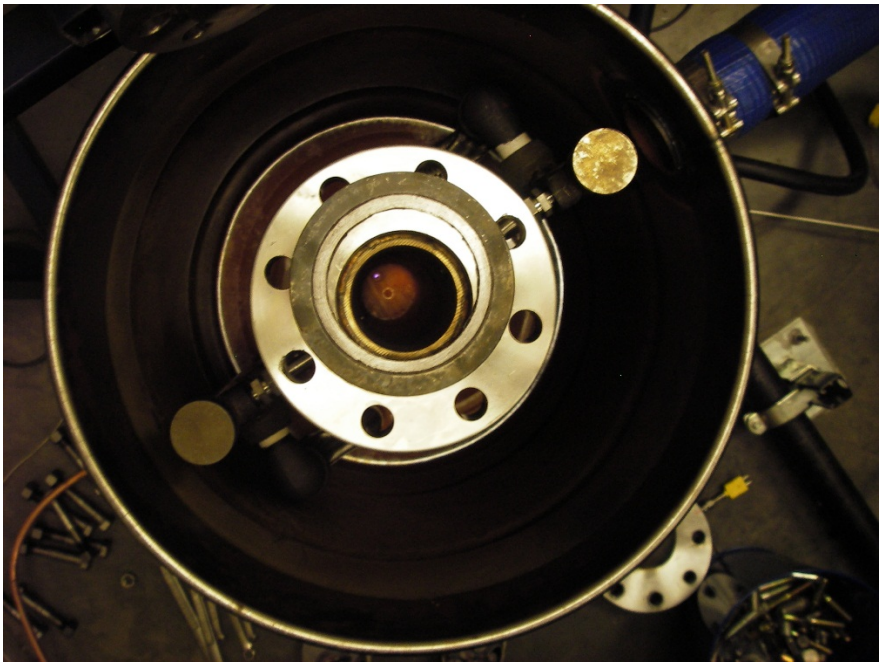

Figure 21: Hydrogen torch with vitiator open to lab.

The oxygen that is to be delivered to the burner must be handled very carefully. Past around 350 psi, pure oxygen has the ability to burn stainless steel. Everything in the oxygen line must be kept very clean, so that small particles cannot be picked up and slammed into tubing walls. Each impact has the potential to create a point of ignition. Compressed gas authorities have set upper limits for the pressures that common piping, tubing, and component materials can be exposed to. As much of the oxygen piping to the burner as possible was made from copper and brass, because of their excellent resistance to oxygen attack[8].

3.4 Cooling

To cool the vitiator, it was placed in a large drum, seen in Figure 22. Water is pushed through an inlet in the bottom of the drum, and forced upwards to an outlet. Even the bottom plate of the vitiator is kept cool by suspending the vitiator on spacers which allowed water to flow across it.

Figure 22: Vitiator in its drum, and fuel cell vessel.

3.5 Pressure Control

The vitiator needed to be lit at nearly atmospheric pressures, and brought up to the operating pressure. It was also desired for the equivalence ratio of the burner to remain constant as the pressure was brought up. Instead of using mass flow controller, it was decided to use a dome-loaded regulator in series with a choked orifice for each gas. A dome-loaded regulator uses a signal pressure, rather than a hand dial, to set its pressure.

A diagram of the piping and instrumentation for the rig can be seen in Figure 23. The line coming off of the building high-pressure air pump has a choked orifice to set the mass flow rate of air through the test bed. A signal pressure is sent to dome-loaded regulators on the natural gas, oxygen, and nitrogen lines. A choked orifice is located downstream of each regulator. Because the temperature of the gases and the sizes of the orifices are constant, the flow through the choked orifices is proportional to the upstream pressure. By ensuring that the upstream pressures are all the same, it is possible to have the proportions of the mass flow rates of each gas to each other remain the same at all operating pressures.

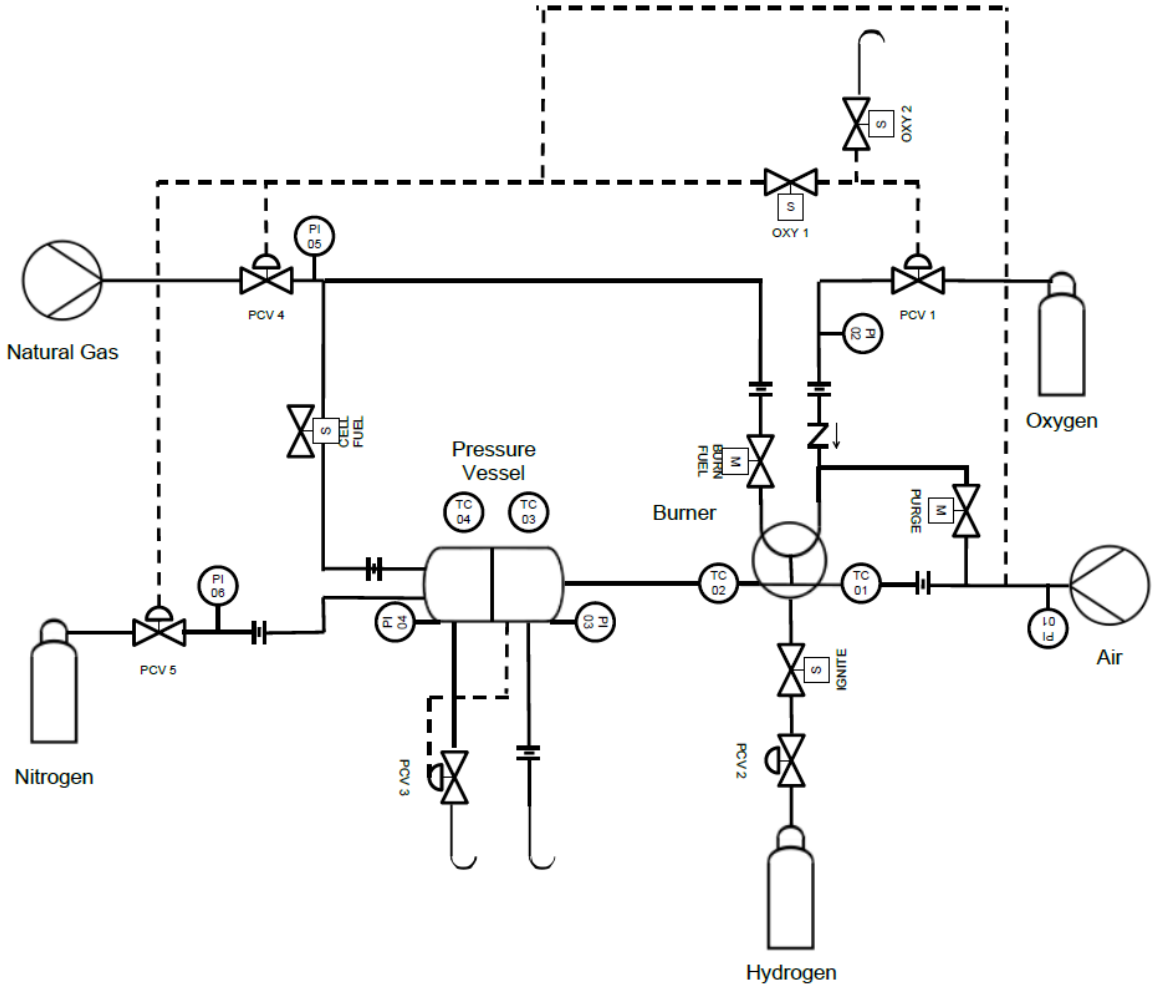

Figure 23: Piping and instrumentation diagram of system.

The pressure in both of the two sections of the pressure vessel needed to be set separately, to prevent the gases from the oxygen-rich side and the oxygen-poor side from mixing. The pressure in the hot air (oxygen-rich) side is set by another choked orifice. This was the only feasible solution given the high temperature of the exhaust gases. The pressure in the methane/nitrogen side was to be set by a dome-loaded back-pressure regulator, using a pressure signal from the air side.

3.6 Data Acquisition and Control

A National Instruments CompactRIO system is used as the data acquisition and control system. The CompactRIO system has several modules which were responsible for different types of data. A thermocouple module is capable of reading 16 separate thermocouples of varying types. An

analog input module is used to read pressure transducer data. An analog output module is capable of outputting 4-20 mA signals to the control valve on the fuel line. A digital output module is used to control relays, which were used to turn solenoids on and off.

The CompactRIO is kept inside of a large enclosure (Figure 24) which has a variety of ports to allow for easy connecting and disconnecting of signal wires. The pressure transducers, which require a separate power source, are handled by a separate, smaller enclosure. The relays are kept in a separate enclosure as well, one which had AC jacks to allow for hassle-free connections. The signal data to and from the other enclosures is carried by D-subminiature cables.

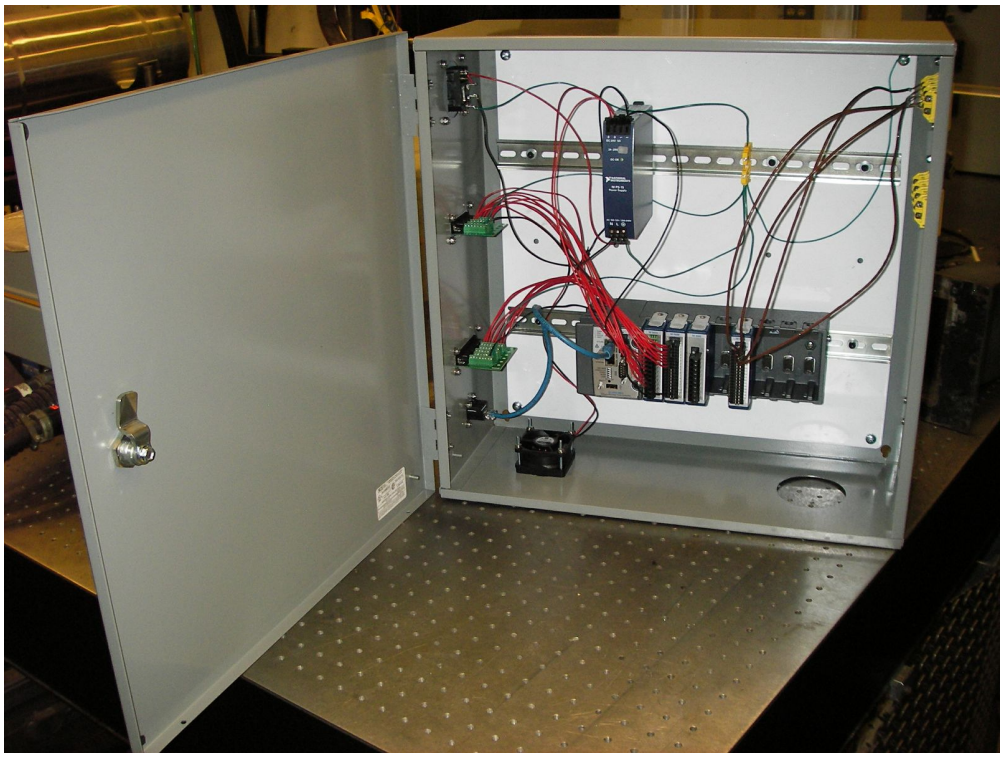

Figure 24: CompactRIO in its enclosure.

3.7 Operation

The operational state of the JTEC testing rig is different from the diagram shown earlier in the report in two respects. First, there is no need for nitrogen or methane to enter the vessel, because there are no fuel cells to inject the methane into. Secondly, the control valve for the vitiator fuel is left out, because it was only desired to exhibit the maximum temperature change the vitiator could produce in the air in the fuel cell vessel.

The operating instructions can be seen in Table 2. Shutdown instructions were not included here for brevity.

Table 2: Setup and operating procedures for testbed.

Setup	1	Turn on room exhaust (Room 130).
	2	Turn on control computer (outside Room 130).
	3	Turn on CompactRIO box, pressure transducer box, and relay box.
	4	Open water valve to cooling drum.
	5	Open Room 130's high-pressure air valve.
	6	Open Room 130's high-pressure natural gas valve.
	7	Open hydrogen bottle in room 130.
	8	Open hydrogen regulator to 30 psig.
	9	Close doors to room.
	10	Extend safety tape across doors.
	11	Turn on high pressure air control box in Room 130's control room.
	12	Bring air pressure to 80 psi.
	13	Turn on high pressure natural gas panel.
	14	Bring natural gas pressure to 300 psi.
Lighting the vitiator	1	Turn on igniter in LabView.
	2	Turn on hydrogen in LabView.
	3	Open oxygen bottle outside room 130.
	4	Wait for temperature at outlet to reach 400 K.
	5	Turn on methane solenoid.
	6	Turn off hydrogen solenoid.
	7	Turn off igniter.
Operation	1	Bring air pressure to desired level.

The LabView interface can be seen in Figure 25. The dome loaded regulators track very well with the signal pressure, so the pressure transducers meant for the oxygen and methane lines are not used. The “Air” signal is the upstream air pressure that is used as the signal pressure for the vitiator gases. The outlet temperature is taken from a thermocouple located at the exit of the vitiator tube. The vessel temperature is from a thermocouple located near the front of the fuel cell vessel. The igniter, hydrogen, and methane buttons are on/off switches. The “stop” button, a LabView standard, will shut off all inputs and outputs to the CompactRIO, thereby shutting off the igniter and all of the solenoids.

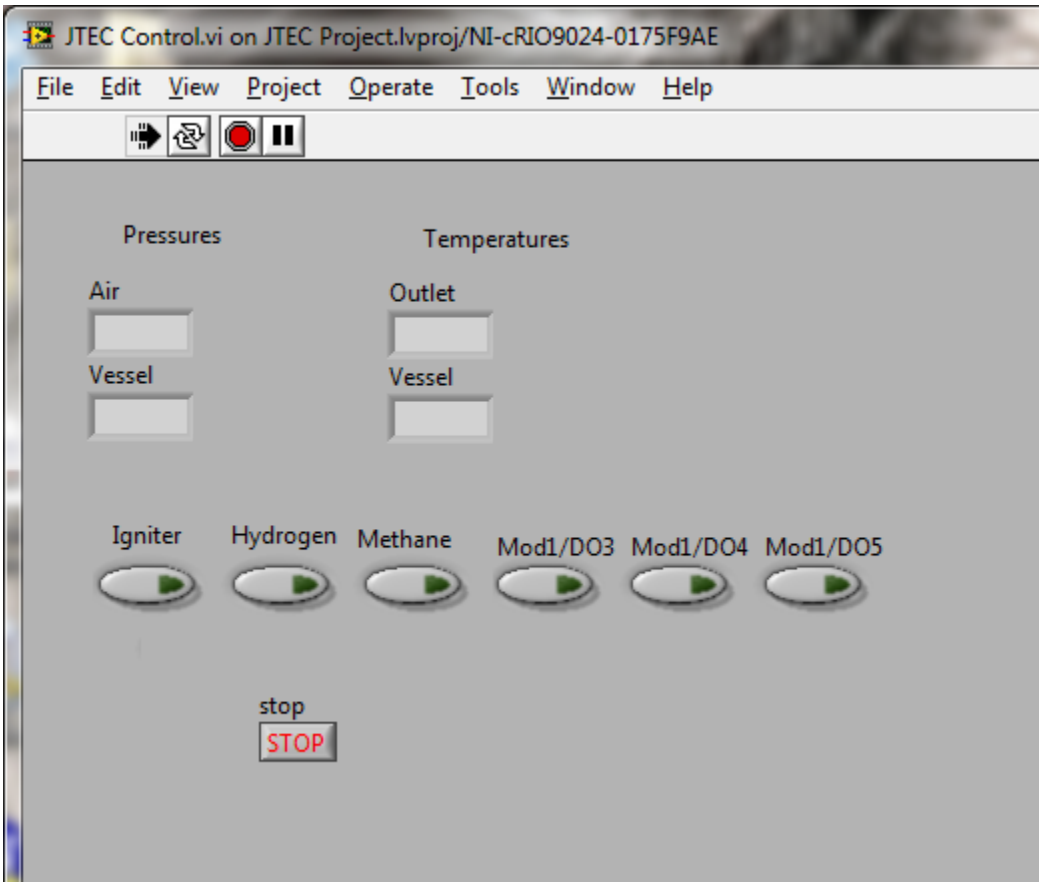

Figure 25: Labview interface for JTEC

Figure 26 shows the LabView interface during the latest test with the JTEC testbed. A pressure of 130psig, or 10 atmospheres, was achieved in the vessel. An outlet temperature of 798 K was produced.

Although this fell well short of the temperature that was desired, there was an easy avenue available for improvement. The building high pressure air heater was not very effective at the low flow rates, only producing an inlet temperature of about 400 Kelvin. This was well short of the 750K it had been known to produce for other rigs. With more time, a bypass of the control system, to bring hotter air into the room, could have been devised. It is also possible that by running the building air heater for a half an hour or more before running, that a better temperature could have been achieved. As it was, the vitiator was able to heat the air by 400 K, and could have reached the target temperature if the building air heater could have provided 600 K air. However, given the lack of fuel cells to test thee additional redesign and effort were deemed unnecessary.

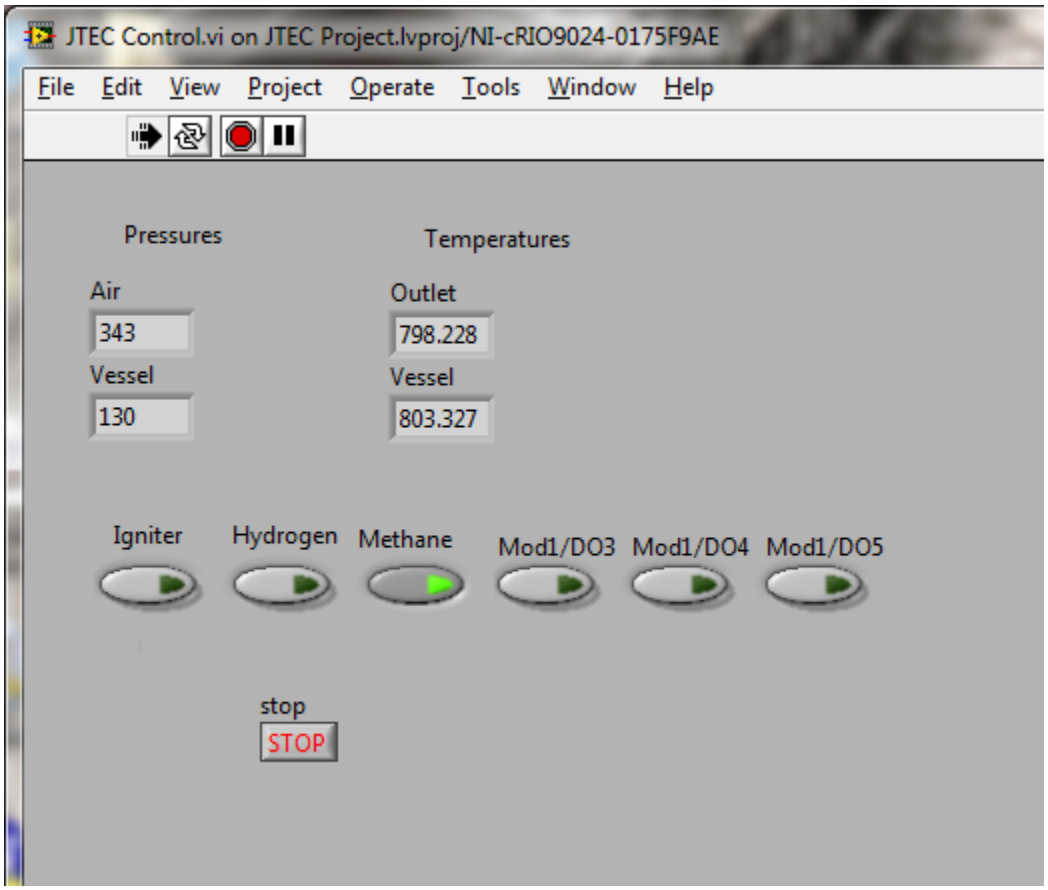

Figure 26: Labview virtual instrument for JTEC at maximum operating temperature.

4 CONCLUSION

Although the project did not end with a test of the proposed fuel cells, some important preliminary work was done that would prove useful if electrical power generation of this kind is ever considered for supersonic combusting aircraft in the future. The thermodynamic model of the supersonic combustor used by the Georgia Tech researchers has shown that the ideal location for the fuel cells is in the back corner of the cavity. The approach used here could also be adapted for combustors of other designs, as well.

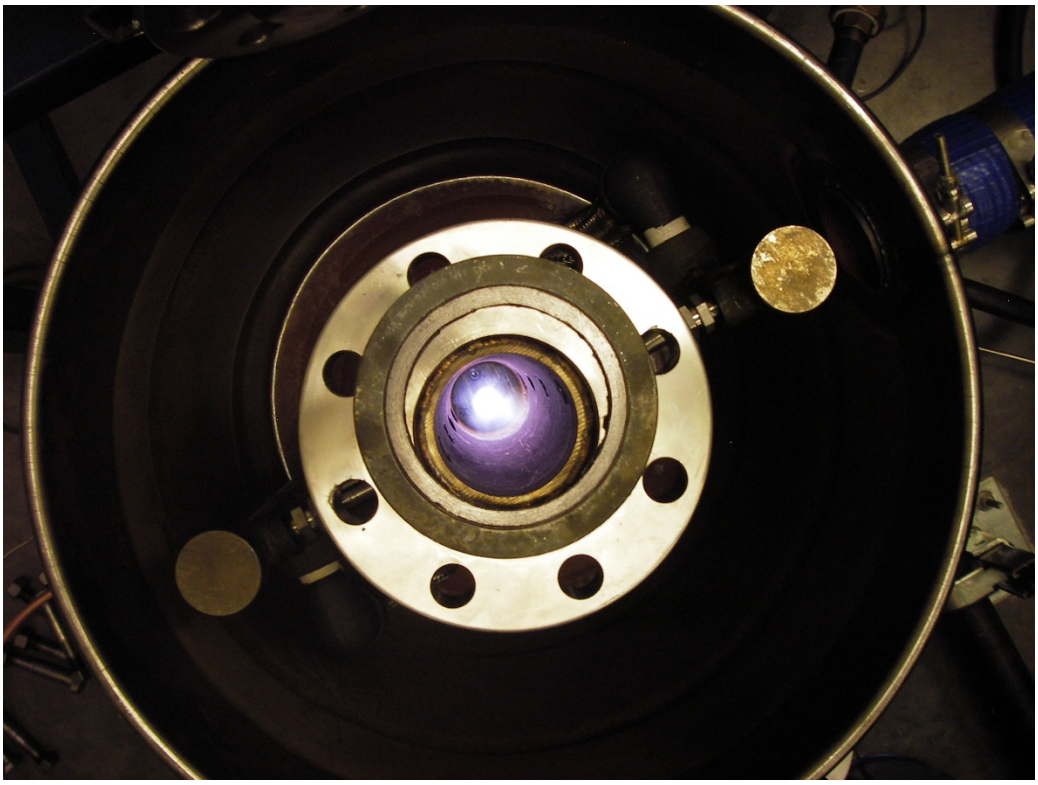

Figure 27: Oxy-methane burner, with vitiator opened to lab.

4.1 References

1. Turns, Stephen R. An Introduction to Combustion: Concepts and Applications. London: McGraw-Hill, 2006.
2. Choi, J. J., Ghodke, C., Menon, S., "Large-Eddy Simulation of Cavity Flame – Holding in a Mach 2.5 Cross Flow," AIAA paper 2010-414, Jan. 2010.
3. Anderson, John D., Hypersonic and High-Temperature Gas Dynamics, Reston, VA: American Institute of Aeronautics and Astronautics, 2006.
4. White, Frank M. Viscous Fluid Flow. New York: McGraw-Hill, 1974.
5. Bertin, J. J., Hypersonic Aerothermodynamics, Washington, DC: American Institute of Aeronautics and Astronautics, 1994.
6. Meader, W.E., and Smart, M.K., "Reference Enthalpy Method Developed from Solutions of the Boundary-Layer Equations," AIAA Journal, Vol. 43, No. 1, 2005, pp. 135-139.
7. Van Driest, E.R., "Problem of Aerodynamic Heating," Aeronautical Engineering Review, Vol. 15, No. 10, 1956, pp. 26-41.
8. European Industrial Gases Association. *Oxygen Pipeline and Piping Systems.* IGC Doc 13/12.